Journal of the Ceramic Society of Japan 132 [2] 39-44 2024
DOI https://doi.org/10.2109/jcersj2.23140

JCS-Japan

FULL PAPER

Ion-exchange and antibacterial properties of layered silicate, Na-kenyaite, prepared using amorphous silicon dioxide (a-SiO_2) blocks

Kuda Durayalage Sulasa Devi Ariyapala[1], Withanage Isuru Udakara Withanage[1], Kosuke Takimoto[1], Nobuhiro Kumada[1,†], Takahiro Takei[1], Norio Saito[1] and Hideharu Horikoshi[2]

[1]Center for Crystal Science and Technology, University of Yamanashi, 7–32 Miyamae, Kofu 400–8511, Japan
[2]TOSO SGM, 4555 Kaisei-cho, Shunan, Yamaguchi 746–0006, Japan

Na-kenyaite, a layered silicate, was synthesized via the hydrothermal method at 190 °C for 24 h using amorphous SiO_2 blocks as a starting material. Changes in the thermal structure of Na-kenyaite were investigated using the in situ high-temperature synchrotron X-ray diffraction data. Na-kenyaite was dehydrated at 200 °C, and its crystal structure was maintained from 200 to 700 °C despite its low crystallinity. It finally decomposed and crystallized to cristobalite via α-quartz. Na-kenyaite was ion-exchanged with Ag^+ and Cu^{2+} ions in different ratios (Ag/Si = 0.01–0.077 and Cu/Si = 0.009–0.044), and the antibacterial properties of the ion-exchanged compounds were evaluated using gram-negative [*Escherichia coli* (*E. coli*)] and gram-positive [*Staphylococcus aureus* (*S. aureus*)] bacteria. Ion-exchanged compounds exhibited an increasing bactericidal effect when the ion-exchange ratios of the compounds increased owing to the release of metal ions with antibacterial properties from the host material. The antibacterial activity of the ion-exchanged compounds was compared based on the relative antibacterial activity, calculated using the inhibition zone obtained after two days of incubation. Cu-kenyaite exhibited better antibacterial activity than Ag-kenyaite against *E. coli* and *S. aureus*.

Key-words : Hydrothermal reaction, Layered silicate, Ion-exchange, Antibacterial property

[Received August 24, 2023; Accepted November 7, 2023]

1. Introduction

Novel low-cost inorganic antibacterial agents must be developed via simple environment-friendly methods for various antibacterial applications. Bacteria are becoming antibiotic resistant and may cause infections that are difficult to treat using existing antibacterial agents. Therefore, the demand for low-cost antibacterial materials has increased in several industries. Some metal ions such as Ag^+, Cu^{2+}, Zn^{2+}, and Mn^{2+} exhibit antibacterial properties and are less toxic to the human body in specific amounts.[1),2)] Therefore, the intercalation of small amounts of these metal ions into inorganic materials has recently received significant attention.[3)–6)] Interestingly, some cations in the interlayer spaces of inorganic layered compounds can be ion-exchanged with metal ions for diverse applications.[7)–9)] Kenyaite is an alkaline silicate that can be categorized into a layered alkali silicate group together with other minerals such as magadiite, octosilicate, kanemite, maketite, ilerite, and RUB-18.[10)–13)] Mineral kenyaite was discovered in concretions together with magadiite and quartz from the lake beds of Lake Magadi, Kenya in 1967.[14)] Both magadiite ($Na_2Si_{14}O_{29}·nH_2O$) and kenyaite ($Na_2Si_{22}O_{45}·nH_2O$) are layered polysilicates in which the interlayer spaces are occupied by sodium ions and water molecules and are composed of SiO_4 tetrahedra.[11)] Pure and well-crystallized Na-kenyaite can be synthesized by optimizing the synthesis conditions and control the transformation between Na-magadiite and Na-kenyaite.[11)] Compared with magadiite, kenyaite has received little attention, and few studies have reported its synthesis.[11),15),16)] The crystal structure of Na-kenyaite was determined by Marler et al. (2021).[17)] This compound has been used as a precursor to prepare porous silicates by pillaring,[18)] conversion into the corresponding acidic form with silanol groups for coupling with a silylating agent to provide an organofunctionalized material,[19)] and intercalation.[20),21)] Although Ag^+-ion-exchanged kenyaite has been tested against gram-negative [*Escherichia coli* (*E. coli*)] bacteria,[22)] there have been no reports on the antibacterial behavior of Ag^+-ion-exchanged kenyaite against gram-positive bacteria and Cu^{2+}-ion-exchanged kenyaite against gram-negative or gram-positive bacteria. Different kenyaite forms have been synthesized using alkali sources such as K-kenyaite, Na-kenyaite, and Rb-kenyaite.[23)] Synthesis of Na-kenyaite has been carried out using laboratory grade feedstock components like colloidal silica, fumed silica or silica gel as the primary silica source in previous reports.[11),19),23)] Our work is a new effort to substitute these pristine sources with discarded by-products from the glass industry, and embark on a journey towards a greener, more

† Corresponding author: N. Kumada; E-mail: kumada@yamanashi.ac.jp

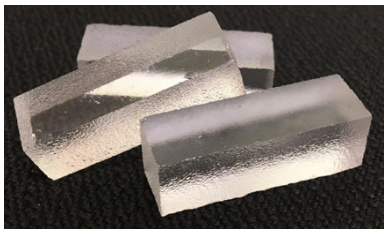

Fig. 1. Starting material (a-SiO_2 blocks).

sustainable and economically viable approach to material synthesis. Additionally, we reported that magadiite, which has a layered structure similar to Na-kenyaite, could not prepared from amorphous silicon dioxide blocks, but from amorphous silicon dioxide fine powder (<500 µm).[24] On the course of this investigation, it is valuable to indicate that Na-kenyaite can be prepared by amorphous silicon dioxide blocks. In this study, we used amorphous SiO_2 blocks (industrial waste supplied by TOSO SGM Co., Ltd.) as the silicon source (**Fig. 1**) for the synthesis of Na-kenyaite. Na-kenyaite was ion-exchanged with Ag^+ and Cu^{2+} ions, and the antibacterial properties of the obtained compounds were investigated. The potential incorporation of metal ions with antibacterial properties into the interlayer of Na-kenyaite allowed for controllable antibacterial activity. These antibacterial compounds can be used in utensils, fabrics, and medical and healthcare products.[25),26)]

2. Experimental

Na-kenyaite was synthesized via the hydrothermal method at 190 °C for 24 h in a Teflon-lined autoclave. The starting materials were amorphous silicon dioxide blocks (a-SiO_2, Fig. 1), which were high purity ones synthesized using $SiCl_4$, and metal impurities (Li, Na, K, Mg, Ca, Al, Cu, Fe) were less than 0.01 ppm and OH was approximately 1000 ppm. These blocks and a 30 mL solution of sodium hydroxide (NaOH) were put into an autoclave with a SiO_2:NaOH molar ratio of 1:0.1. The product was filtered, washed with distilled water, and dried at 60 °C for 24 h. After ion-exchange with $AgNO_3$ and $Cu(NO_3)_2$ at room temperature, the mixture was stirred with 100 mL of distilled water for 24 h. The mole ratios of M: kenyaite in the ion-exchanged compounds ranged from 0.1 to 3 [M = $AgNO_3$ or $Cu(NO_3)_2$]. Finally, the ion-exchanged compounds were filtered, washed with distilled water, and dried at 60 °C for 24 h.

The compounds were identified by X-ray powder diffraction (XRD) (Rigaku, MiniFlex 600) using Ni-filtered Cu $K\alpha$ radiation ($\lambda = 0.15418$ nm). The crystal structure of Na-kenyaite was determined using the VESTA software package.[27)] High-temperature synchrotron XRD measurements at a heating rate of 80 K min^{-1} were performed using BL02B2 powder diffraction beamline at SPring-8, Hyogo, Japan. The morphologies of the compounds and their chemical compositions were determined using scanning electron microscopy (SEM) (HITACHI Miniscope TM3030) and energy-dispersive X-ray spectrometry. Thermal behavior of the compounds was investigated using

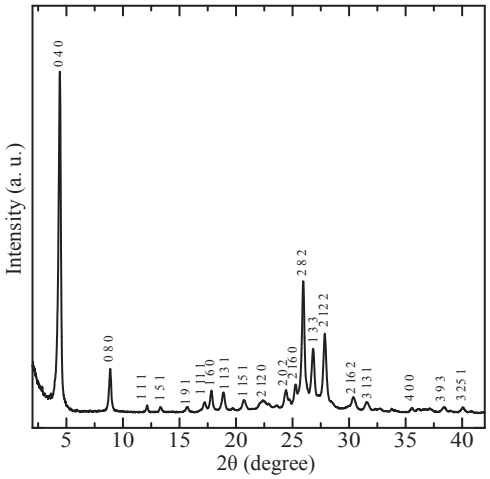

Fig. 2. Powder XRD pattern of Na-kenyaite (ICSD No. 135046).

thermogravimetry-differential thermal analysis (TG–DTA) (Rigaku Thermo Plus) at a heating rate of 10 °C min^{-1}.

Antibacterial properties were evaluated using the inhibition zone method. Two bacterial strains, gram-negative (*E. coil*, NBRC 3972) and gram-positive [*Staphylococcus aureus* (*S. aureus*), NBRC 12732] bacteria, were used as model bacteria and were obtained from the National Institute of Technology and Evaluation (NITE), Biological Resource Center (NBRC). Pellets (diameter = 10 mm) were prepared using 0.3 g of powdered compound and sterilized at 160 °C for 90 min. The pellets were then placed in the middle of the agar surface. A mixture of 10^6 CFU/mL bacteria solution (1 mL) and condensed nutrient agar (9 mL) was poured onto the pellets. Subsequently, the solidified agar dishes were maintained at 37 °C for 48 h, and photographs were captured after incubation. The areas of the inhibition circles were measured using ImageJ software (National Institute of Health, MD), and the relative antibacterial activities (RAA) of the compounds were calculated using Eq. (1) to compare the antibacterial efficiencies.

$$\text{Relative antibacterial activity} = (A_2 - A_1)/A_1 \quad (1)$$

(A_1 = area of compound pellet and A_2 = area of inhibition zone).

3. Results and discussion

3.1 Na-kenyaite

The XRD pattern of Na-kenyaite could be indexed to the orthorhombic cell (**Fig. 2**). The calculated lattice parameters are $a = 10.10$ Å, $b = 79.58$ Å, and $c = 10.64$ Å, which agree well with the previously reported values [$a = 10.080(1)$ Å, $b = 79.383(8)$ Å, and $c = 10.604(1)$ Å].[17)] Synthesized Na-kenyaite has a high crystallinity compared to recent studies[28),29)] and the crystal structure of Na-kenyaite[17)] was determined using the VESTA software package.[27)] As shown in **Fig. 4**, this crystal structure is described as a layered structure with a basal spacing of 19.7 Å

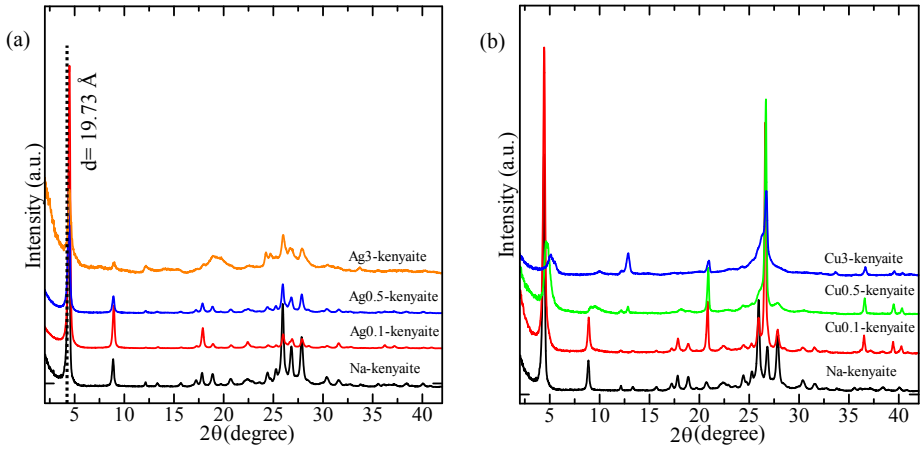

Fig. 3. (a) Powder XRD patterns of Na-kenyaite and silver ion exchanged samples and (b) copper ion exchanged samples.

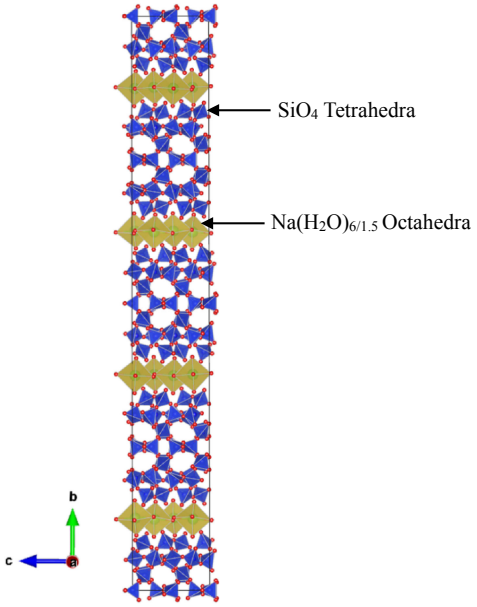

Fig. 4. Structure of kenyaite drawn by using VESTA software.

and silicate layers with thickness of 15.9 Å (ignoring the van der Waals radii for the terminal oxygen atoms) along the *b*-axis. In the interlayer space, the Na atoms are present as mutually interconnected [$Na(H_2O)_{6/1.5}$] octahedra. The water molecules form hydrogen bonds with the oxygen atoms of the silanol groups at the edges of the tetrahedral silicate layer.[17] With agreeing to previous reports[17),28),29)] this compound has a plate-like morphology and agglomerates into a rosette-like shape with a size of approximately 10 µm, as shown in the SEM image in **Fig. 5**(a). **Figure 6** shows the in situ high-temperature synchrotron X-ray diffraction patterns at 1100 K. As shown in **Fig. 7** a mass loss of 8.96 % is observed in the TG curve corresponding to the three endothermic peaks below 200 °C in the DTA curve. This is attributed to the removal of water molecules adsorbed on the surface of Na-kenyaite (up to 100 °C) and bound to Na^+ in the interlayer (100–200 °C). A successive mass loss of 2.5 % occurs above 300 °C, which is assigned to the dehydroxylation of the silicate structure.[11),30)] In the temperature range of 500–900 K, a weak peak corresponding to the basal spacing is observed, indicating that the crystal structure of kenyaite is retained. Kenyaite decomposes and crystallizes into quartz at 700 °C and subsequently into cristobalite at temperatures above 830 °C.

3.2 Ion-exchange with Ag^+ and Cu^{2+}

The powder XRD patterns of the as-synthesized Na-kenyaite, ion-exchanged Ag-kenyaite and Cu-kenyaite are shown in **Fig. 3**. The SEM images of Na-kenyaite and ion-exchanged compounds (Fig. 5) show that the particle shape and size do not significantly change during the ion-exchange reactions. These results indicate that the ion-exchange reaction does not affect the crystal structure of kenyaite. **Table 1** summarizes the A/Si ratios (A = Na, Ag, or Cu) of the ion-exchanged compounds. The 040 diffraction peak at $2\theta = 4.48°$, corresponding to the basal spacing of 19.73 Å, increases to 19.82 Å for Ag3-kenyaite and decreases to 17.52 Å for Cu3-kenyaite after the ion exchange. When the ion-exchange degree increases, this peak becomes broader and less intense because of the non-homogeneous ion-exchange of Na^+ ions with larger Ag^+ ions or smaller Cu^{2+} ions ($r_{Na+} = 1.16$ Å, $r_{Ag+} = 1.28$ Å, and $r_{Cu2+} = 0.87$ Å). This morphology is maintained during the ion-exchange reaction. For Cu-kenyaite, this peak is considerably broader than that for Ag-kenyaite, indicating that the Ag^+ ion exchange is more homogeneous than the Cu^{2+} ion exchange. These ion-exchange properties of kenyaite align with the findings of previous studies by Z. A. M. Kebir et al. (2018)[22)] and H. Fatima et al. (2022).[28)]

3.3 Antibacterial properties

The antibacterial activity was evaluated by measuring the inhibition zone and pellet area using the photographs obtained after incubation with bacteria. The ImageJ software was used to calculate the areas. **Figures 8** and **9** show the inhibition results of Ag-kenyaite and Cu-kenyaite against *E. coli* and *S. aureus* after 48 h of incubation,

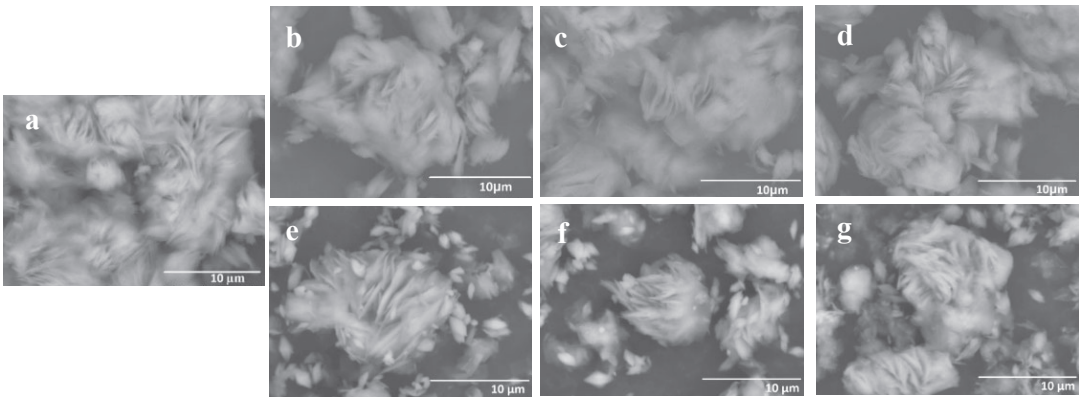

Fig. 5. SEM images of (a) Na-kenyaite, ion exchanged samples of (b) Ag0.1-kenyaite, (c) Ag0.5-kenyaite, (d) Ag3-kenyaite, (e) Cu0.1-kenyaite, (f) Cu0.5-kenyaite and (g) Cu3-kenyaite.

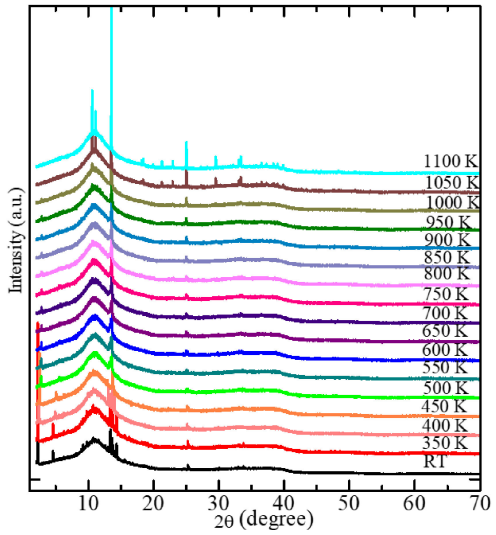

Fig. 6. Structural transformation of Na-kenyaite from room temperature to 1100 K.

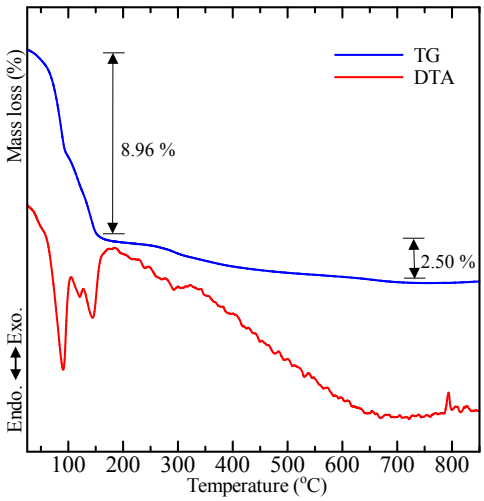

Fig. 7. TG–DTA curve of Na-kenyaite.

respectively. Na-kenyaite does not show any inhibition circle owing to the absence of antibacterial properties. The Ag^+- and Cu^{2+}-ion-exchanged compounds exhibit antibacterial properties against *E. coli* and *S. aureus*. The RAA of the Ag^+- and Cu^{2+}-ion-exchanged compounds was calculated using Eq. (1); the composition dependence is shown in **Fig. 10**.

Table 1. Ion composition of ion-exchanged samples

Sample	A/Si ratio
Na-kenyaite	0.091
Ag0.1-kenyaite	0.01
Ag0.5-kenyaite	0.017
Ag1-kenyaite	0.026
Ag2-kenyaite	0.072
Ag3-kenyaite	0.077
Cu0.1-kenyaite	0.009
Cu0.2-kenyaite	0.018
Cu0.3-kenyaite	0.025
Cu0.5-kenyaite	0.035
Cu3-kenyaite	0.044

A = Na, Ag or Cu.

There are some reports[31),32)] on the higher antibacterial activity of Ag^+ ions. However, in this study, Cu^{2+}-ion-exchanged kenyaite exhibits higher antibacterial activity than Ag^+-ion-exchanged kenyaite. The diffusion of Cu^{2+} ions onto the agar surface is visible in blue after incubation, indicating the contribution of Cu^{2+} ions to the antibacterial properties. Cu-kenyaite exhibits stronger antibacterial activity against *E. coli* than that against *S. aureus*. Similar bacterial behavior of copper has been reported in Cu^{2+}-ion-exchanged $KHSi_2O_5$ compounds[31)] and Cu^{2+}-ion-exchanged zeolites ($Na_2Al_2Si_{2.5}O_9{\cdot}6.2H_2O$).[32)] In this study, Cu-kenyaite shows the highest RAA against *E. coli* and *S. aureus* at 3.68 and 2.87, respectively, whereas Cu-$KHSi_2O_5$ exhibits the highest values of 3.47 and 2.81, respectively. Valodkar et al. (2011)[33)] reported that Cu could inhibit bacterial growth more than Ag against gram-negative and gram-positive bacteria. They suggested that the continuous release and slow diffusion of metal ions from nanoparticles might lead to antibacterial behavior. Furthermore, according to Heidenau et al. (2005),[34)] Cu-filled TiO_2 coatings show outstanding antibacterial properties compared to silver and several other metal ions. Demirci et al. (2014)[32)] reported that the required inhib-

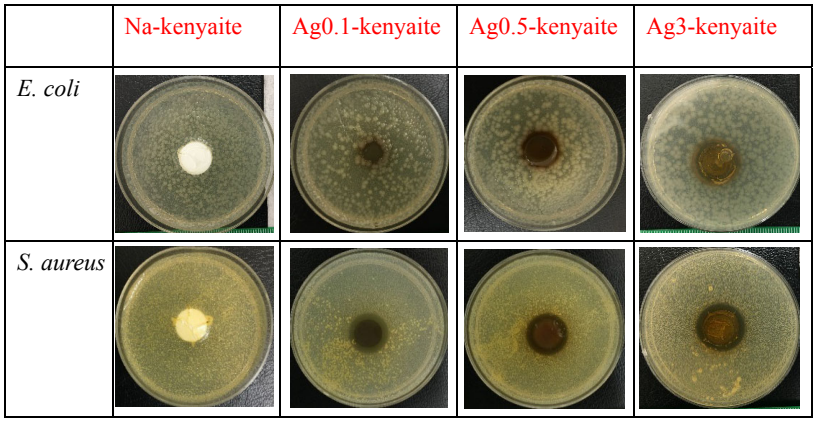

Fig. 8. Images of the inhibition results of Na-kenyaite and Ag-kenyaite samples against *E. coli* and *S. aureus* after 48 h incubation.

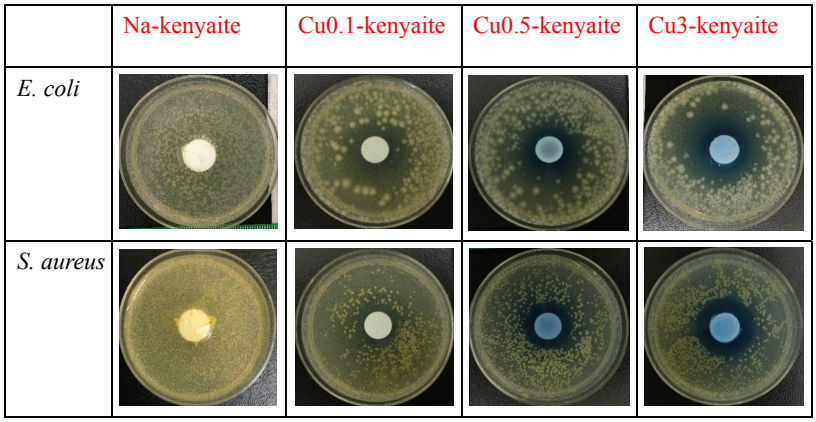

Fig. 9. Images of the inhibition results of Na-kenyaite and Cu-kenyaite samples against *E. coli* and *S. aureus* after 48 h incubation.

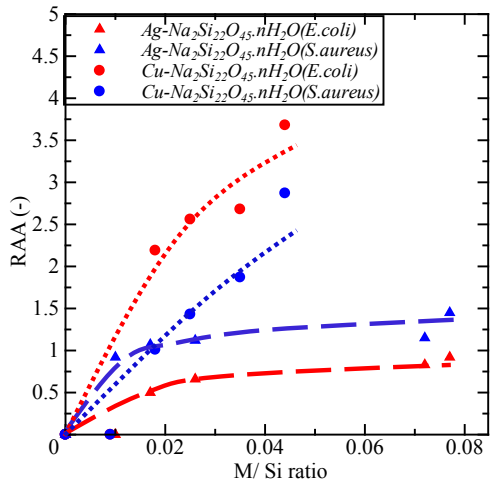

Fig. 10. RAA with M/Si ratio of Ag-kenyaite and Cu-kenyaite against *S. aureus* and *E. coli* (M = Ag or Cu).

itory concentration of Cu^{2+}-ion-exchanged zeolite against *E. coli* was significantly lower (256 µg/mL) than that against *S. aureus* (1024 µg/mL), resulting in a moderate antibacterial effect. Morphological changes in gram-negative and gram-positive bacteria were responsible for these inhibitory differences. *E. coli* possesses a thin bacterial cell wall with a more negatively charged and rigid surface than *S. aureus*.[35] Cu^{2+} ions released by the layered structure can combine with the bacterial cell wall by electrostatic attraction and rupture it, resulting in an intracellular ion imbalance, leakage of DNA and RNA, and protein disorganization in the bacterial cell.[36] Additionally, bactericidal processes occur in the peptidoglycan of the cell wall of *S. aureus* and the outer membrane of the cell wall of *E. coli* because of the generation of Cu^{2+}-ions-induced reactive oxygen species (O_2^-, ·OH, OH^-) and H_2O_2, causing oxidative stress and leading to bacterial death.[37]

In contrast to Cu-kenyaite, Ag kenyaite exhibits higher RAA against *S. aureus* (1.45) than *E. coli* (0.92). Similar bacterial behavior of Ag has been reported in Ag^+-ion-exchanged $KHSi_2O_5$, Ag^+-ion-exchanged pyrochlore-type potassium niobate/potassium tantalate, and Ag^+-ion-exchanged zeolite ($Na_2Al_2Si_{2.5}O_9 \cdot 6.2H_2O$).[31),32),38)] In this study, the areas of the inhibition zones increase with an increase in the Ag^+ ion content, indicating a controllable antibacterial property of the ion-exchanged kenyaite. When Ag^+ ions are released from the host kenyaite structure, they are attracted to the negatively charged bacterial

cell wall via electrostatic forces and destroy it. These Ag^+ ions can enter the cell, causing cytoplasmic shrinkage, DNA condensation, loss of replication ability, and inactivation of proteins that interrupt the enzymatic activity in the cell.[39] The antimicrobial mechanism of Ag^+ ions can lead to cell damage and bacterial death.

4. Conclusions

Na-kenyaite was synthesized via the hydrothermal method using industrial waste SiO_2 blocks. The as-synthesized Na-kenyaite was successfully ion-exchanged with different ratios of Ag^+ and Cu^{2+} in an aqueous medium at room temperature. Cu^{2+}-ion-exchanged kenyaite exhibited better antibacterial activity than Ag^+-ion-exchanged kenyaite. Both Ag^+- and Cu^{2+}-ion-exchanged compounds exhibited increasing bactericidal activity when the ion-exchange ratios were increased, imparting controllable antibacterial properties to the ion-exchanged kenyaite compounds. These properties of kenyaite would allow its commercial use in the biomedical and healthcare industries.

Acknowledgement Experiments at SPring-8 were performed with the approval of the Japan Synchrotron Radiation Research Institute (Proposal No. 2021B1008).

References

1) E. Pazdziora, K. Matějová, M. Valášková, S. Holešová and M. Hundáková, Proc. 2nd Int. Conf. NANOCON, Oct. 12–14, Olomouc, Czech Republic (2010) pp. 10–14.
2) W. L. Du, S. S. Niu, Y. L. Xu, Z. R. Xu and C. L. Fan, *Carbohyd. Polym.*, **75**, 385–389 (2009).
3) I. Withanage, N. Kumada, T. Takei, S. Yanagida, Y. Kuroiwa and C. Moriyoshi, *J. Ceram. Soc. Jpn.*, **125**, 776–778 (2017).
4) W. I. U. Withanage, N. Kumada, T. Takei, S. Yanagida, K. Tadanaga, A. Miura, N. C. Rosero-Navarro and M. Azuma, *J. Ceram. Soc. Jpn.*, **128**, 46–50 (2020).
5) N. Torkian, A. Bahrami, A. Hosseini-Abari, M. M. Momeni, M. Abdolkarimi-Mahabadi, A. Bayat, P. Hajipour, H. A. Rourani, M. S. Abbasi, S. Torkian, Y. Wen, M. Y. Mehr and A. Hojjati-Najafabadi, *Environ. Res.*, **207**, 112157 (2022).
6) C. H. Hu, Z. R. Xu and M. S. Xia, *Vet. Microbiol.*, **109**, 83–88 (2005).
7) W. I. U. Withanage, S. Yanagida, T. Takei and N. Kumada, *J. Ceram. Soc. Jpn.*, **126**, 784–788 (2018).
8) T. Takei, K. Sekijima, D. Wang, N. Kumada and N. Kinomura, *Solid State Ionics*, **170**, 111–115 (2004).
9) N. Kumada, M. Takeshita, F. Muto and N. Kinomura, *Mater. Res. Bull.*, **23**, 1053–1060 (1988).
10) G. G. Almond, R. K. Harris and K. R. Franklin, *J. Mater. Chem.*, **7**, 681–687 (1997).
11) F. Kooli, L. Mianhui and J. Plevert, *Clay Sci.*, **12**, 25–30 (2006).
12) L. A. J. Garvie, B. Devouard, T. L. Groy, F. Cámara and P. R. Buseck, *Am. Mineral.*, **84**, 1170–1175 (1999).
13) W. Schwieger, P. Werner and K. H. Bergk, *Colloid Polym. Sci.*, **269**, 1071–1073 (1991).
14) H. P. Eugster, *Science*, **157**, 1177–1180 (1967).
15) K. Kosuge, A. Yamazaki, A. Tsunashima and R. Otsuka, *J. Ceram. Soc. Jpn.*, **100**, 326–331 (1992).
16) O. Kwon, S. Jeong, J. Suh and J. Lee, *B. Korean Chem. Soc.*, **16**, 737–741 (1995).
17) B. Marler, I. Grosskreuz and H. Gies, *J. Solid State Chem.*, **300**, 122215 (2021).
18) B. Aicha, S. Mohamed, M. B. Jocelyne, L. Benedicte, B. Jean-Luc and B. Abdelkader, *J. Porous Mat.*, **25**, 801–812 (2018).
19) B. Royer, N. F. Cardoso, E. C. Lima, V. S. O. Ruiz, T. R. Macedo and C. Airoldi, *J. Colloid Interf. Sci.*, **336**, 398–405 (2009).
20) R. M. Kosanke, *Clay Sci.*, **37**, 37–46 (1997).
21) H. Muraishi, *Clay Sci.*, **36**, 22–34 (1996).
22) Z. A. M. Kebir, M. Adel, M. Adjdir, A. Bengueddach and M. Sassi, *Mater. Res. Express*, **5**, 085021 (2018).
23) F. Feng and K. J. Balkus, *J. Porous Mat.*, **10**, 5–15 (2003).
24) N. Saito, N. Kumada, T. Takei and H. Horikoshi, *J. Ceram. Soc. Jpn.*, **131**, 488–490 (2023).
25) J. Inkinen, R. Mäkinen, M. M. Keinänen-Toivola, K. Nordström and M. Ahonen, *Lett. Appl. Microbiol.*, **64**, 19–26 (2017).
26) X. Liu, T. Lin, B. Peng and X. Wang, *Text. Res. J.*, **82**, 584–590 (2012).
27) K. Momma and F. Izumi, *J. Appl. Crystallogr.*, **41**, 653–658 (2008).
28) H. Fatima, J. D. Seo, J. Kim and M. Park, *J. Porous Mat.*, **29**, 111–117 (2022).
29) Z. Feng, Y. Wang, T. Lv, S. Zhang, X. Liu, X. Liu and C. Meng, *Solid State Sci.*, **103**, 106196 (2020).
30) K. Beneke and G. Lagaly, *Am. Mineral.*, **68**, 818–826 (1983).
31) K. D. S. D. Ariyapala, W. I. U. Withanage, N. Kumada, T. Takei and H. Horikoshi, *J. Ion Exchange*, **33**, 112–117 (2022).
32) S. Demirci, Z. Ustaoğlu, G. A. Yilmazer, F. Sahin and N. Baç, *Appl. Biochem. Biotech.*, **172**, 1652–1662 (2014).
33) M. Valodkar, S. Modi, A. Pal and S. Thakore, *Mater. Res. Bull.*, **46**, 384–389 (2011).
34) F. Heidenau, W. Mittelmeier, R. Detsch, M. Haenle, F. Stenzel, G. Ziegler and H. Gollwitzer, *J. Mater. Sci.-Mater. M.*, **16**, 883–888 (2005).
35) H. Ikigai, T. Nakae, Y. Hara and T. Shimamura, *BBA-Biomembranes*, **1147**, 132–136 (1993).
36) X. Cai, B. Zhang, Y. Liang, J. Zhang, Y. Yan, X. Chen, Z. Wu, H. Liu, S. Wen, S. Tan and T. Wu, *Colloid Surface B*, **132**, 281–289 (2015).
37) T. Ishida, *Virol. Immunol. J.*, **1**, 1–8 (2017).
38) W. I. U. Withanage, K. D. S. D. Ariyapala, N. Kumada, T. Takei, M. Ueda and M. Aizawa, *J. Asian Ceram. Soc.*, **10**, 49–57 (2022).
39) Q. L. Feng, J. Wu, G. Q. Chen, F. Z. Cui, T. N. Kim and J. O. Kim, *J. Biomed. Mater. Res.*, **52**, 662–668 (2000).